Original Article

ISSN: 2349 - 4891

International
Journal of Recent Research and Applied Studies
(Multidisciplinary Open Access Refereed e-Journal)

Damage and energy absorption behaviour of low-velocity impacted fibre-reinforced composite panels using analytical and data filtering techniques

Umar Farooq[1] and Peter Myler[2]

[1]Reader, Department of Engineering, Support and Advance Sciences, University of Bolton, Bolton BL3 5AB UK

[2]Professor, Head of Engineering, Support and Advance Sciences, University of Bolton, Bolton BL3 5AB UK

Received 15st March 2021, Accepted 1st April 2021

Abstract

This work reports low-velocity impact-induced damage and energy absorption predictions of carbon fibre-reinforced laminated composite panels using analytical and data filtering techniques. Flat nose low-velocity impact of fibrous composite panels inflicts barely visible impact damage that could result in unexpected catastrophic failure that is a major concern to the aerospace industry. Extensive studies are being conducted to improve damage resistance and damage tolerance and energy absorption capabilities of the structures to prevent such failures. Previous studies on the topic revealed that load-deflection based approach works well for the onset of damage. However, flat nose impacts of relatively thick laminates produce level off load-deflection curves once certain displacement energy is reached. A very little information is available to extract serious damages from the leveled off loads. Thus, the analytical and data filtering approach was employed to quantify the energy absorbed by different mechanisms during flat and round nose impacts of 8- and 16-Ply laminates. Moreover, advanced data filtering techniques were applied to characterize load thresholds and absorbed energies from the leveled off curves. Comparisons of the results showed that the energy-based approach was more suitable for the determination of the initiation, propagation, accumulation, and extent of internal damage modes. The information could useful to be utilised at pre-design development and analysis.

Key words: *Fibre-reinforced composite panels, Low-velocity impact, Absorbed energy.*

I. Introduction

Fibrous composite panels are being extensively used as building block of many kinds of aircraft components. Because they exhibit better impact resistance, higher amount of impact energy absorption, design flexibility for damage tolerant systems subjected to extreme changes in pressure, temperature and strain rates [1]. However, wings and fuselage of an aircraft are exposed to tool and tool-box drops during service life that might result in catastrophic failures. Extensive studies are being conducted on varies aspects of the topic to save human lives, capital assets, and avert the failure. Among them, Caprino et al. [2] have performed low velocity impact tests on panels of different thicknesses. They have examined the force and absorbed energy at the onset of delamination, the maximum force and related energy, and threshold energy. Some experimental investigations have been carried out by Hosur et al. [3] to determine the response of four different combinations of hybrid laminates subjected to low velocity impact loading.

Correspondence
Umar Farooq
Reader, Department of Engineering, Support and Advance Sciences, University of Bolton, Bolton BL3 5AB UK

Datta et al. [5] have investigated the effects of variable impact energy and laminate thickness on the low velocity impact damage tolerance of composite laminates. Mitrevski et al. [6] studied the effect of impactor shape on the drop-weight impact performance of thin woven carbon/epoxy composites. They concluded that specimen absorbed more energy when impacted by a conical impactor while hemispherical impactors produced highest contact force and lowest contact time. The approach based on impact force is applied when the onset of damage has to be determined for different plate or impactor geometries while energy-based approach could be more helpful in examining the extent of damage. Many works presented semi-empirical formulae for predicting impact characteristics such as peak force, contact duration, and peak strain on back surface. Some simple, but efficient theoretical and energy-based approximation methods have also been presented to deal with damage characterisation and extent of the other relevant parameters [7-12]. Relatively reliable energy balance for impact of laminates includes three major energy terms: the energy stored elastically, the energy absorbed in creation of matrix damage and the energy absorbed in creation of fibre damage. There are also two smaller terms: the energy for permanent indentation and a system loss term. Damage in the forms of matrix cracking, delamination, and fibre breakage were included and analyzed. Results including the force history and delamination areas were found to correlate well with the

ISSN: 2349 – 4891

experiments [10]. However, common difficulty in measuring data, analysis, and damage detection is the contamination of noise due to vibration of impactor, target, rig, and other apparatus at different frequencies [10-18]. Damage detections in impacted composite laminates using de-noising and frequency response methods, and de-noising the impact produced data and damage detection by means of electrical potential techniques are reported in [17]. The studies report that the impact produced noise could amplify and distort data interpretation and analysis. It has been reported that three-dimensional elasticity theory based finite element analysis combined with the low velocity impact tests could reduce the noise. Further studies to reduce the difficulty with data analysis based on coupled finite element and Kalman filter can be seen in [19-24]. A new sigma-point (linear regression based) Kalman filter was proposed to address nonlinearities induced by inter-laminar lay-ups. The filter uses the first order Taylor series expansion and accordingly updates statistics of the structural state. Improved estimates on delamination state and parameter identification via joint Kalman linear statistical filters, and similar other works are reported in [25-28].

In the previous works, the damage states of the laminates were characterized as a function of impactor mass and energy where energy balance was used to correlate damage and impact conditions. The aim of this paper is to complement the studies, and quantify the relationship between the damage mechanisms and energy absorption, as a function of time, displacement and impactor energy. Relatively more energy terms: energy stored elastically, energy absorbed by permanent indentation, energy absorbed by matrix damage, energy absorbed by fibre damage. Impact energy absorptions together with the material damage characteristics of the panels were investigated. The behaviour is presented in forms of the curves of contact force-displacement as absorbed energy, energy-time history, and images of damages specimens. Damage modes and the damage processes under varied impact energies versus energy absorptions were considered to determine extent of damage. The area approximated under load-deflection curve for flat nose impactor is found to be larger than that of the round nose impactor. The absorbed energy provides expected estimates of accumulated internal damage modes: indentation, matrix cracks, and de-bonding/delamination for impacts with round and flat nose impactor profiles.

1 Test laminates and material properties

Geometrical properties were proposed in [10] with the laminates of code Fibredux 914C-833-40. In-plane dimensions of the laminates were 150 mm x 120 mm with variable thicknesses. Fibres, matrix, ply with fibre orientations, laminate with test area, components, and aircraft are shown in **Figure 1(a)-(f)**. Panels considered consist of

a) 8-Ply laminates (average thickness: 2.4 mm) consisted of lay-ups code $[0^0/90^0/45^0/\text{-}45^0]_S$
b) 16-Ply laminates (average thickness: 4.8 mm) of code $[0^0/90^0/45^0/\text{-}45^0]_{2S}$

Test area is consisting of circular cut-outs of 50 mm diameter**.**

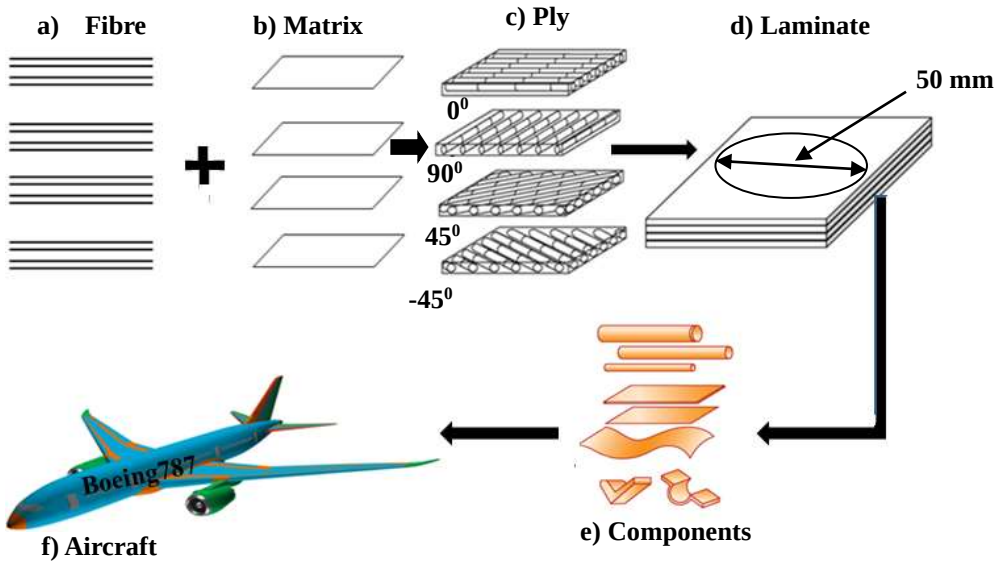

Figure 1: Schematics of a) fibres, b) matrix, c) ply, d) circular cut-out, e) components, and f) aircraft

Accidental foreign object impact on laminates could be of any shape. Nonetheless, two possible nose shapes of harden stainless steel considered herein. Round and flat nose impactors have shank of diameter 20 mm. The flat and round nose shape impactors used were made of harden stainless steel. Both impactors have shank of diameter 20 mm. The shank reduces to 107(±0.18) mm for the ground flat impact face. The round nose shape impactor has radius of 57(±0.15) mm. No catastrophic failures or complete penetrations were assumed. The drop-weight models were investigated for range of velocity 1.6 to 4.5 m/s selected on the basis of the experimental results proposed by James [1]. Test samples along with prescribed material properties were provided by the industry, and the same were used in experimental investigation [10]. All plies were assumed to be of uniform material properties and thickness as shown in **Table 1.**

Table 1: Properties of laminate and impactor **[10]**

Property	Units	Fibredux T300
Tensile Modulus (E_{11})	GPa	230
Tensile Modulus ($E_{22} = E_{33}$)	GPa	21
In-plane Shear Modulus ($G_{12=} G_{13}$)	GPa	88
Out-of-plane Shear Modulus (G_{23})	GPa	11
Poisson's Ratio (ν_{12})	-	0.2
Longitudinal Tensile Strength (X_T)	MPa	650
In-plane Shear Strength (S_{12})	MPa	180
Longitudinal Compressive Strength (Y_T)	MPa	650
Transverse shear strength ($S_{13} = S_{23}$)	MPa	32
Inter-laminar shear strength (Z_T)	MPa	10

2 The drop-weight impact tester

The INSTRON^{TM} Dynatup 9250 HV drop-weight impact tester is widely used for simulating local damage of 'real world scenario' such as accidentally falling dropped hammer, tool (box) during assembly or maintenance as well as accidental hit of low speed kitchen/loading unloading vans to the wing or fuselage of an aircraft. The salient features of the testing machine has a maximum drop height of maximum 1.2 metres equipped with an impactor, a fine transducer with capacity 22.24 kN, high bandwidth digital signal processing electronics, and data acquisition software. Round and flat nose shape impactor made of steel and consisting of three parts: the crosshead, shank, and nose were used. A non-standard purpose-built flat nose impactor was manufactured from hardened steel in the laboratory (the Composite Research Laboratory of Bolton University). As, the flat type impact is regarded common danger in aerospace industry hence particularly emphasized in this study. Both the impactors have shank of diameter 20 mm reducing to 10 ± (0.18) mm with the round impactor having a nose shape radius of 5 ± (0.15) mm and flat impactor a ground flat impact face. The total mass of the chosen impactor was 4.96 Kg (included impactor mass and crosshead). Prior to impacting, the laminate was tightly clamped around end boundary anvils are fixtures that hold specimens during testing clamped by using the bolts. The target holder sandwiches laminate between two rectangular steel plates that had circular central holes (for 50 mm diameters test area). The same fixture and impact affected area (50 mm diameter) at central region were considered for all the test cases as shown in **Figure 2**. All tests were performed at room temperature. Experiments restricted to the analysis of low velocity below than 5 m/s to avoid penetration. The sample size, supported mode and impactor size were made mostly following the American Standard Testing Method **(ASTM: D7136)**. The methods is accepted as standard testing method for measuring damage resistance of a fibre-reinforced polymer matrix composite to a drop weight impact event. For each type of impactor least three tests were performed for every coupon.

ISSN: 2349 – 4891

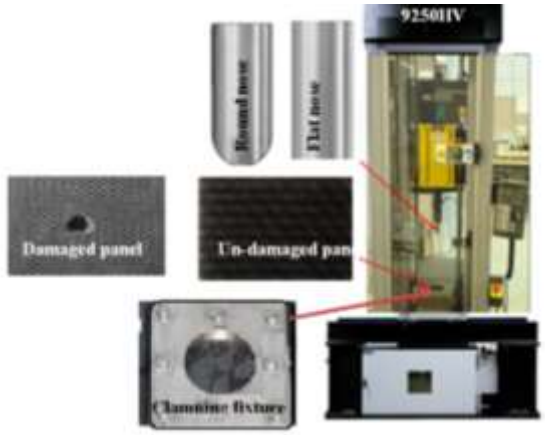

Figure 2: Schematic of INSTRON™ 9250HV tester

In the drop weight system, the potential energy of the system is converted into kinetic energy during an impact onto the specimen. After the impactor dropped, the initial impact velocity is calculated from the distance between two edges on the time trigger and the time interval they passes through the sensor. The velocity of the impactor head first touches the specimen was adjusted/calculated from conversion of potential energy into kinetic energy depends on the impactor's drop height and mass. After the impact begins, the contact forces at many consecutive instances were detected by the force transducer attached to the impactor. The force history data was recorder by data acquisition system. Data points collected during a test are up to 16000 for each channel. Acceleration of the impactor is obtained by dividing difference between impact forces a total weight of the impactor (gM_{total}) to the total weight of the impactor deflection derives from a double integration of acceleration of the impactor. The ratio of the energy absorbed by the specimen to the impact energy carried by the impactor is used as the measure of the specimen's energy absorption performance, which give total energy to damage/failure determined by the difference in pre- and post-test potential energies of the impact tup. The electromagnetic braking system stopped the impactor after rebound, preventing repeated impact energy on the target. All tests followed the same procedures.

3 Theoretical determination of impact parameters

There are many theoretical aspects that must be considered for the extended interpretation of experimentally produced test data. The level of the impact energy or momentum is changed by varying the drop height of the impactor. This has the effect of changing both the impact energy and the impact velocity simultaneously. The analytical impact parameters are useful tool to get fast predictive results for an unknown parameter from mathematical relations using known parameters for a given impact configuration. These models are usually developed to predict the response of the system until damage onset, which is sufficient to compare different impact cases with different values of the governing parameters. All recorded data generated from the impact tests were used to calculate other unknown values. The main constraints on the theoretical formulations were that the all deformations were in the elastic region. The use of test generated data in place of more costly impact testing have been utilised to calculate other unknown parameters. From the experimentally measured/known parameters such as load, velocity, displacement, energy other theoretical aspects were considered for any possible relations. The parameters estimated with experiment are used to determine the other possible parameters useful to correlate and estimate impact damage and damage mechanism.

4.1 Parameters that affect the impact response

The parameters that affect the impact response can be classified into three different groups: structural parameters, impactor parameters and environmental conditions. Parameters such as impact energy shape, thickness, size, material properties, ply stacking sequence, and boundary conditions are categorized as structural parameters. Impactor parameters comprise shape, diameter, material properties, weight, angle of incidence and impact velocity. As under the same impact energy, the structural parameters, impact energy shape, size and boundary conditions affect the impact response significantly. For example, a small plate is stiffer than a large plate which results in a larger impact force on the small plate. So, the relationship between impact force and damage area was used instead of that between impact energy and damage area as that means there was no need to consider plate size and other effects. The research results paved the way that a small piece of test specimen can be used to simulate impact damage in a large in-service structure when the same impact force was employed. At the same time impactor geometry severely affects the impact damage of a plate. Theoretically determined impact parameters can be correlated to:

a) impact energy – kinetic energy of the impactor;
b) peak force – maximum force recorded during the impact event;
c) critical force – threshold force for onset of delamination;
d) critical energy – impact energy analogous to critical force;
e) dissipated energy – energy absorbed in damage initiation and propagation

4.2 Relationship of actual and virtual work to absorbed kinetic energy

Acceleration (a) in free fall can be measured directly and weight can be measured independently by the deflection of a spring. Forces (F) generally vary during an impact

ISSN: 2349 – 4891

but masses m remains constant. Newton's second law of motion says

$$\boldsymbol{F = ma} \quad (1)$$

If mass of the impactor is to vary, keeping the velocity constant the following parameters can be calculated using the Newton law:

$$\boldsymbol{F = mg - f = m\frac{dv}{dt}} \quad (2)$$

The contact force $F(t)$ during the impact load depends on the impactor mass m and velocity v. Initial impactor velocity v_0 depends on the free fall acceleration g and downfall height h:

$$\boldsymbol{v_0 = \sqrt{2gh}} \quad (3)$$

The velocity (v_0) at the impact point allows the forces generated during test together with deflection and energy to be recorded using the formulations:

$$\boldsymbol{v = v_0 + gt - \frac{1}{m}\int_0^t f dt} \quad (4)$$

$$\boldsymbol{x = v_0 t + \frac{1}{2}gt^2 - \frac{1}{m}\int_0^t \int_0^t f dt} \quad (5)$$

Multiplying Eq. (4) by $\int_0^t f dt$

$$\boldsymbol{E = v_0 \int_0^t f dt + g\int_0^t f t dt - \frac{1}{m}\left[\int_0^t f dt\right]^2} \quad (6)$$

The impact duration (t) can also be determined from Eq. (5), and work done is defined as a force (F) multiplied by a displacement differential ($\boldsymbol{dx}$):

$$\boldsymbol{W = \int F\, dx} \quad (7)$$

D'Alembert's principle can be obtained from Eq. (7) assuming limiting case:

$$\boldsymbol{Fdx = ma\, dx} \quad (8)$$

Replacing acceleration by the approximate velocity in Eq. (8) gives

$$\boldsymbol{Fdx = mv\,\frac{dv}{dx}dx = mv\, dv} \quad (9)$$

The Eq. (9) can be used for both actual and virtual work. The work done equals the energy released which is more convenient to relate the work done to the absorbed energy. For potential energy 'V' this relationship can be expressed as $\delta W = \delta V$. From Eq. (7) the relation can be expressed as $F = -\frac{dV}{dx}$. Kinetic energy is possessed by a mass as a result of its velocity, and it equals the work needed to bring the mass up to this velocity or down if loses its velocity. The relationship can be derived from D'Alembert's principle by integration both sides

$$\boldsymbol{\int_{x_1}^{x_2} Fdx = \int_{v_0}^{v_f} mvdv} \quad (10)$$

As with potential energy, it is convenient to relate the work done to the kinetic energy T with the absorbed energy of the moving body ($\delta W = -\delta T$). This can be expressed as $F = -\frac{dT}{dx}$ that is related to the kinetic energy**:**

$$\boldsymbol{\int_{x_1}^{x_2} Fdx = \int_{T_1}^{T_2} dT} \quad (11)$$

This leads to correlate the impact energy transferred from the impactor to the target and absorbed by the each failure mechanisms of the fraction of impact energy. The experimental impact force measured during the impact event makes possible to evaluate the impact energy, which reaches the target as well as absorbed energy and the elastic energy.

4.3 Relationship of kinetic energy to absorbed energy

From experimental measurements, number of other useful parameters can be calculated utilising the mathematical formulations. The general energy expression for an impact event may be generally broken into elastic and inelastic contributions. The elastic deformations consist of tup and crosshead (impact and rebound), test fixture (base and guide columns), contact-flexural, shear, and membrane. The inelastic deformations could be micro-matrix cracking, delamination/de-bonding, fibre breakage, tower vibration, damping, and structural influences**.** To control all those forms make the analysis almost impossible. Luckily, many of these energy absorbing mechanisms are negligible in their contributions. Those of obvious importance are the elastic plate deformations and contact deformations. A linear-elastic response (plate bending and contact) up to incipient damage is assumed and the point of interest at which damage begins. It is desirable to avoid plastic and non-linear effects which occur after this point because of the complexities in modelling them and, therefore, predicting them. The area under the load-time curve is called impulse and expressed as $\int \mathbf{F}\, \boldsymbol{dt}$**.** This gives energy absorbed during the impact even as

$$\boldsymbol{E = \int_{t_0}^{t_f} Fvdt} \quad (12)$$

Where F is the instantaneous load and v is the instantaneous velocity recorded during impact, t_0 is the time of initial impact, usually taken as zero, and t_f is the time for completion of impact. The apparent absorbed energy Eq. (12) can be re-written as

$$\boldsymbol{E = v_0 \int_{t_0}^{t_f} Fdt} \quad (13)$$

A close approximation to the actual energy can be obtained by replacing the instantaneous velocity v_0 Eq. (13) with the average velocity '$\bar{v}$' as

$$\boldsymbol{E = \bar{v} \int_{t_0}^{t_f} Fdt} \quad (14)$$

A useful feature of the moment is that it is always conserved. Impulse-moment balances are used mainly in situations in which the duration of the forces is so short that no significant displacement occurs before it is over. Using the relation between impulse, $\int F\, dt$, and momentum, $m(v_0 - v_f)$ and approximating the average velocity as $\frac{(v_0+v_f)}{2}$, the average velocity in terms of the initial velocity can be obtained by

$\boldsymbol{I = \int_0^t F dt = m(v_0 - v_f)}$ as

$$\boldsymbol{mv_f = mv_0 - \int_0^t F dt} \quad (15)$$

multiplying Eq. (15) by v_0 gives

$$\boldsymbol{mv_f v_0 = mv_0 v_0 - v_0 \int_0^t F dt} \quad (16)$$

or

$\boldsymbol{v_f m \frac{v_0^2}{v_0} = mv_0^2 - E_a}$ or

$$\boldsymbol{v_f \frac{2E_0}{v_0} = 2E_0 - E_a} \quad (17)$$

Hence, the average velocity can be written as

$$\boldsymbol{\bar{v} = v_0 \left(1 - \frac{E_a}{4E_0}\right)} \quad (18)$$

Therefore, maximum energy available during impact of the tup in terms of kinetic energy just prior to impact is the measured impact energy. Combining Eq. (14) and (18) gives

$$\boldsymbol{E = E_a \left(1 - \frac{E_a}{4E_0}\right)} \quad (19)$$

The instantaneous absorbed energy E_{ab} can be determined:

$$\boldsymbol{E_{ab}(t) = \frac{1}{2} m v_0^2 - \frac{1}{2} m \left(v_0 - \left(\frac{1}{m}\right) \int_0^t F(t) dt\right)^2} \quad (20)$$

After the impact, the impactor velocity gradually decreases as the laminate absorbs the impact kinetic energy:

$$\boldsymbol{E_{imp} = \frac{1}{2} m v^2} \quad (21)$$

The other forms of energies involved in the system: elastic potential energy and energy due to the external transverse load are formulated. The energy stored in a laminate of length L, width b under vertical load is considered. Bending is given by

$$\boldsymbol{E_{bend} = \frac{1}{2} \int_{y=0}^{y=b} \int_{x=0}^{x=b} \left[D_{11} \left(\frac{\partial^2 w}{\partial x^2}\right)^2 + 2D_{12} \frac{\partial^2 w}{\partial x^2} \frac{\partial^2 w}{\partial y^2} + D_{22} \left(\frac{\partial^2 w}{\partial y^2}\right)^2 + \left(D_{16} \frac{\partial^2 w}{\partial x^2} + D_{26} \frac{\partial^2 w}{\partial y^2}\right) \frac{\partial^2 w}{\partial x \partial y} + 4D_{66} \left(\frac{\partial^2 w}{\partial x \partial y}\right)^2 \right] dx dy} \quad (22)$$

Where w is the transverse displacement of the laminate. The matrix coefficients D_{ij} are the components of the bending stiffness matrix, x is the coordinate along the length of the plate, and y is the coordinate along the width of the plate. The energy stored by mid-plane (membrane) stretching is given by

$$\boldsymbol{E_{mem} = \frac{1}{2} \int_{y=0}^{y=b} \int_{x=0}^{x=b} \left[\frac{A_{11}}{2} \left(\frac{\partial w}{\partial x}\right)^4 + (A_{12} + 2A_{66}) \left(\frac{\partial w}{\partial x} \frac{\partial w}{\partial y}\right)^2 + \frac{A_{22}}{2} \left(\frac{\partial w}{\partial y}\right)^4 \right] dx dy} \quad (23)$$

Whereas: A_{ij} are components of the extensional stiffness matrix.

The energy stored due to externally applied load, $N_{x,}$ is given by

$$\boldsymbol{E_{Nx} = \frac{1}{2} \int_{y=0}^{y=b} \int_{x=0}^{x=L} \left[N_x \left(\frac{\partial w}{\partial x}\right)^2 \right] dx dy} \quad (24)$$

The energy put into the system by the transverse load, F, is given by

$$\boldsymbol{E_F = -\int_{y=0}^{y=b} \int_{x=0}^{x=b} \left[\frac{4F}{Lb}\right] dx dy} \quad (25)$$

The total energy of the system is given by

$$\boldsymbol{E_{tot} = E_{bend} + E_{mem} + E_{Nx} + E_F} \quad (26)$$

Assuming that the impactor velocity is zero at the maximum deflection, the work done by the contact force along the loading curve is equal to the initial kinetic energy E_0 of the impactor:

$$\boldsymbol{E_0 = -\int_0^{\delta_{max}} F \, d\delta} \quad (27)$$

Where the plate deflection δ is taken equal to the impactor displacement and the gravitational force is neglected. Analogously, the impactor kinetic energy E_T at the end of the impact even is: lost by the impactor is:

$$\boldsymbol{E_T = -\int_{\delta_{max}}^{\delta_T} F \, d\delta} \quad (28)$$

Then the amount of kinetic energy lost by the impactor is:

$$\boldsymbol{\Delta E_T = E_0 - E_T = \int_0^{\delta_{max}} F \, d\delta + \int_{\delta_{max}}^{\delta_T} F \, d\delta}$$

$$\boldsymbol{= \int_0^{\delta_T} F \, d\delta} \quad (29)$$

This means that the impactor energy loss is thus the area enclosed by the complete load-deflection curve. According to the law of energy conservation, Eq. (29) is equivalent to the following equation based on the impulse balance:

$$\begin{cases} \boldsymbol{m(v_0 - v_T)} & = \int_0^T F dt \\ \boldsymbol{\Delta E_0} & = \frac{1}{2} m (v_0^2 - v_T^2) \end{cases} \quad (30)$$

whereas v_T is the impactor velocity at time *T*.

In an arithmetical point of view, Eq. (30) is more desirable for energy loss calculations. The equation needs one integration evaluation while Eq. (29) needs two. The Eq. (29) gives the relationship between the load deflection behaviour and the impactor energy loss. That

equation is applicable for energy analyses that are not on a time basis. To understand those experimental observations thoroughly, the analytical solutions for the delamination development are needed. The impact absorption efficiency is defined as the absorption energy divided by area density of the material. By subtracting the dissipated energy from the total impactor kinetic energy a closer estimate of the actual peak force can be made [27]. The impact velocity can be determined from energy relations. Assuming the absorbed energy Eq. (6) and Eq. (20) $(\boldsymbol{E_{ab}(t)})$ as change in the strain energy ΔU that equates to the change in kinetic energyΔE_{imp}, presented as

$$\Delta \boldsymbol{U} = \int_{t_n}^{t_n+\Delta t} \boldsymbol{F v}\, \boldsymbol{dt} \quad (31)$$

$$\Delta \boldsymbol{E_{imp}} = \frac{1}{2}\boldsymbol{m}\left(\boldsymbol{V_n^2} - \boldsymbol{V_{n+1}^2}\right) \quad (32)$$

Solving Eq. (31) and (32), the impact velocity Eq. (4) can be written as

$$\boldsymbol{V_{n+1}} = \sqrt{\boldsymbol{V_n^2} - \frac{\boldsymbol{2.F.V_n\Delta t}}{\boldsymbol{m}}} \quad (33)$$

After receiving the velocity data, the change of the strain energy could be automatically calculated with velocity, impact force, and impact time. The experimental impact force measured during the impact event makes possible to evaluate the impact energy, which reaches the target as well as absorbed energy and the elastic energy. Using modified Simpson's rule based on second-order polynomial, the Eqns. (11), (20), and (28) can be numerically integrated as:

$$\int_a^b \mathbf{F}\boldsymbol{dx} \approx \frac{1}{3}\left[\left(\mathbf{F}(\mathbf{a}) + \mathbf{F}(\boldsymbol{b})\right) + \mathbf{2}\sum_{k=1}^{n/2-1}\mathbf{F}(\boldsymbol{x_{2k}}) + \mathbf{4}\sum_{k=1}^{n/2}\boldsymbol{F}(\boldsymbol{x_{2k-1}})\right] \quad (34)$$

Where: the interval [a (lower limit), b (upper limit)] is split up in n sub-intervals, with n an even number where equidistant x values are x_0, x_1, ..., x_n, the step width being $h = \frac{b-a}{n}$. The method is simple and efficient to predict absorbed energy. Peak force can be determined by assuming a linear elastic response (very simple case) the peak force data can be fitted by the empirical power law curve whereby

$$F_{peak} = \sqrt{2kE_{imp}} \quad (35)$$

In contrast to the delamination threshold force model Eq. (35), the multiple delaminations reduce the bending stiffness of the laminate to zero within the damage zone. However, the membrane stiffness remains unchanged as the load-carrying fibres preserve their properties and orientations. The energy releases due to the area enlargement of a virtual membrane. The stiffness K_d^m of the virtual membrane is derived from the large deflection solution for a clamped isotropic circular plate under a point load F in Timoshenko [34]:

$$\boldsymbol{F} = \frac{\boldsymbol{16\pi D w_0}}{\boldsymbol{a_0^2}} + \frac{\boldsymbol{K_m E h w_0^3}}{\boldsymbol{a_0^2}} \Rightarrow \boldsymbol{K_d^m} = \frac{\boldsymbol{3\pi K_m E h w_0^2}}{\boldsymbol{A}} \quad (36)$$

Where w_0 is the maximum deflection of the circular plate, h is the plate thickness, a_0 is the plate radius, the A is the plate area and D is the plate bending rigidity. E is the engineering effective in-plane modulus of the original laminate, which has been assumed to be equal to the average modulus of the delaminated sub-laminates. The factor K_m is very sensitive to the boundary conditions. For a clamped plate with immovable edge, the K_m value is equal to 2 approximately. For a clamped plate with edge free to move, the K_m value becomes 0.9 approximately. The linearised energy release rate can be written in the following form:

$$\boldsymbol{G} = \frac{1}{2}\boldsymbol{F^2}\frac{\boldsymbol{\partial C_d^m}}{\boldsymbol{\partial A}} = \frac{\boldsymbol{F^2}}{\boldsymbol{6\pi K_m E h w_0^2}} \quad (37)$$

Equating G obtained to a certain constant critical energy release rate G_c for multiple delaminations, the load applied is found to be proportional to the maximum deflection of the circular membrane when the energy balance for delamination propagation is satisfied:

$$\boldsymbol{C} = \boldsymbol{C_u} + \sqrt{\boldsymbol{6\pi K_m E h G_c}} \quad (39)$$

$$\boldsymbol{F} = \sqrt{\boldsymbol{6\pi K_m E h G_c w_0}} \quad (38)$$

This implies that the compliance of the delaminating plate remains constant:

Where C_u is the undamaged structural compliance defined in Eq. (39).

After the delamination propagation curve starts from the knee points $(\delta_{cr},\ F_{cr})$, the expression for the curve can be rewritten as follows:

$$\boldsymbol{F - F_{cr}} = (\boldsymbol{\delta - \delta_{cr}}) * \left(\boldsymbol{C_u} + \frac{\boldsymbol{1}}{\sqrt{\boldsymbol{6\pi K_m E h G_c}}}\right)^{\boldsymbol{-1}} \quad (40)$$

This means that no significant increase in the load F is needed to keep the delamination growing, after the delamination threshold force F_{cr} is exceeded. It is clear that the impactor energy loss is equal to the area enclosed by the complete load deflection curve, while the initial impact energy is the area under the loading curve. This suggests that the relationship between the initial impact energy and the impactor energy loss can be

For brittle composites with a very small G_c value, Eq. (40) can be shown to agree with the D-R model:

$$\boldsymbol{G_c \to 0} \Rightarrow \boldsymbol{F \to F_{cr}} \quad (41)$$

derived from the load deflection curve. The amount of energy lost during the impact event is termed "absorbed energy." Usually the initial impact energy is used to describe the intensity of an impact event. However, the damage development cannot be directly related to the absolute value of the impactor kinetic energy, but to the energy consumed for crack formation, i.e. a part of the kinetic energy that the impactor loses during the impact.

ISSN: 2349 – 4891

By relating the impactor energy loss to the energy absorbed due to delamination development, the delamination area can be proven to be related to the initial energy. On the basis of the experimental observation and the delamination threshold and propagation model, a simplified load deflection curve is assumed for the determination of the impactor energy loss **Figure 3**.The loading curve is represented by two straight lines numbered with 1 and 2. Their slopes $tan\theta_1$and $tan\theta_2$are defined as the undamaged target stiffness *Ku* and the delamination propagation stiffness (K_p) respectively. The knee point is indicated as (δ_{cr}, F_{cr}), and peak load point with (δ_{max}, F_{max}). The unloading curve is assumed to be linear and parallel to the loading curve before the knee point. This line is numbered with 3. The dotted line numbered with 4 is the neglected part of the unloading curve compared with the actual experiments. The numbering in **Figure 3** corresponds with the numbering and the sequence. The plate with no or insignificant delamination deforms into a smooth and doubly curved shape. When the delamination threshold force is reached, delaminations develop to a significant size. The localised material weakening leads to an additional localised deflection that plays an important role in the potential energy release. During the unloading phase, the undamaged region dominates the rebounding motion at the beginning, since the damaged region possesses far insufficient stiffness to rebound. For a comparably small damage region, the rebounding stiffness of the undamaged region can be reasonably approximated by the undamaged stiffness of the structure. This justifies the assumption that the unloading curve is parallel to the first loading curve. The rebounding process of the damaged region involves relatively little deformation energy and is therefore negligible. The loading curve is represented by two straight lines numbered with 1 and 2. Their slopes $tan\theta_1$and $tan\theta_2$are defined as the undamaged target stiffness *Ku* and the delamination propagation stiffness (K_p) respectively. The knee point is indicated as (δ_{cr}, F_{cr}), and peak load point with (δ_{max}, F_{max}). The unloading curve is assumed to be linear and parallel to the loading curve before the knee point. This line is numbered with 3. The dotted line numbered with 4 is the neglected part of the unloading curve compared with the actual experiments. The numbering in Figure 3 corresponds with the numbering and the sequence. The plate with no or insignificant delamination deforms into a smooth and doubly curved shape. When the delamination threshold force is reached, delaminations develop to a significant size. The localised material weakening leads to an additional localised deflection that plays an important role in the potential energy release. During the unloading phase, the undamaged region dominates the rebounding motion at the beginning, since the damaged region possesses far insufficient stiffness to rebound. For a comparably small damage region, the rebounding stiffness of the undamaged region can be reasonably approximated by the undamaged stiffness of the structure. This justifies the assumption that the unloading curve is parallel to the first loading curve. The rebounding process of the damaged region involves relatively little deformation energy and is therefore negligible.

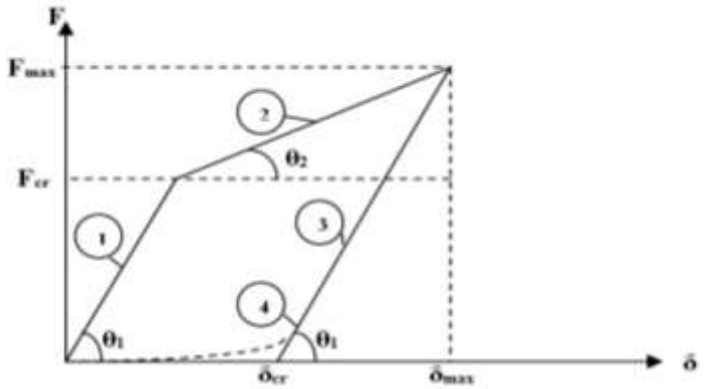

Figure 3: Schematic of simplified load-deflection curve

From Figure 3, the following equations are established:

$$\begin{cases} \boldsymbol{K_u} & = & \frac{\boldsymbol{F_{cr}}}{\boldsymbol{\delta_{cr}}} \\ \boldsymbol{K_p} & = & \frac{\boldsymbol{F_{max}-F_{cr}}}{\boldsymbol{\delta_{max}-\delta_{cr}}} \\ \boldsymbol{E_0} & = & \boldsymbol{\Delta E_0 + \frac{1}{2} F_{cr}\delta_{cr}\left(\frac{F_{max}}{F_{cr}}\right)^2} \\ \Rightarrow \boldsymbol{E_0} & = & \boldsymbol{\frac{1}{2} F_{cr}\delta_{cr} + \frac{1}{2}(F_{max}+F_{max}) * (\delta_{max}-\delta_{cr})} \end{cases} \quad (42)$$

Whereas E_0 is the incidental impact energy and ΔE_0 is the kinetic energy loss of the impactor. Eliminating P_{max} and δ_{max} yield:

$$\boldsymbol{\Delta E_0 = \left(E_0 - \frac{1}{2} F_{cr}\delta_{cr}\right) * \left(1 - \frac{K_p}{K_u}\right)} \quad (43)$$

Eq. (43) shows clearly that the linear relationship between the impactor energy loss ΔE_0 and the incidental impact energy E_0 is based on the identity of shape of the impact load–deflection curves. It can be observed that the load deflection curves from the same series of flat plates and curved panel tests are indeed identical in shape. Based on equations (40) and (43), the theoretical delamination threshold energy E_{cr} and the impact energy transfer factor Γ are defined as follows:

$$\boldsymbol{E_{cr} = \frac{1}{2} F_{cr}\delta_{cr} = \frac{1}{2} F_{cr}^2 C_u} \quad (44)$$

$$\boldsymbol{\Gamma = 1 - \frac{K_p}{K_u} = 1 - \left(\frac{K_u}{\sqrt{6\pi K_m E h G_c}}\right)^{-1}} \quad (45)$$

It is obvious that the parameter Γ can only vary between 0 and 1. A zero energy transfer factor corresponds to $K_p = K_u$ as no damage development implies that can complete restitution of the elastic energy. The maximum energy transfer $\Gamma = 1$corresponds to $K_p = 0$ in the cases of unstable delamination growth.

From the standpoint of a design engineer, it is not convenient to use the peak impact force to calculate the projected delamination area, since both quantities are unknown in the beginning of an impact analysis. However, Eq. (49) is useful to understand effects of the thickness and curvature of composite structures. As the relationship is independent on the global structural stiffness (K_u).

$$\boldsymbol{\Delta E_0 = \Gamma(E_0 - E_{cr})} \quad (46)$$

On the basis of the law of conservation of energy, the greatest part of the impactor energy loss $\Delta E_0$is absorbed due to the damage development. If the average critical energy release rate is constant: $\Delta E_0 = G_c A$, the impact energy $E_0$is linearly related to the projected delamination area:

$$\boldsymbol{A = \frac{\Gamma}{G_c}(E_0 - E_{cr})} \quad (47)$$

Equation (47) shows that the impact damage resistance can be improved by increasing the G_c value of the material. This agrees well with practical experiences [9]. From Eq. (42), an additional relationship can be derived between the projected delamination area and the peak impact force. Eliminating the energy terms $\boldsymbol{E_0}$ and $\boldsymbol{\Delta E_0}$ in Eq. (48)-(47), the damage area can be expressed as follows:

$$\boldsymbol{A = \frac{F_{max}^2 - F_{cr}^2}{2G_c}\left(\frac{1}{K_p} - \frac{1}{K_u}\right)} \quad (48)$$

Based on equations (39) and deflection, Eq. (48) can be rewritten as:

$$\boldsymbol{A = \frac{1}{\sqrt{6\pi K_m\, E h G_c^3}}(F_{max}^2 - F_{cr}^2)} \quad (49)$$

In this way, the projected delamination area has been

5 Results and Discussions

5.1 Absorbed and impact energy for round and flat nose impact profiles

In **Figure 4** and **Figure 5** two sets of data are plotted against impact energy. The strain energy is the energy used in creating damage and the total absorbed energy is the amount of energy used during the impact event, which includes the energy transferred back to the impactor in the form of rebound energy.

Impact energy = total absorbed energy (strain energy + rebound energy + losses during the impact event)+ losses before the impact event.

In both the figures, a linear trend is presented for the total absorbed energy up to full laminate penetration. A total absorbed energy to impact energy ratio of 1:1.11 can be seen indicating a 1J loss in performance per 10J of impact energy before the impact event, which is consistent with the calibration test findings. The point at which the linear response intersects the impact penetration energy could give a crude estimation of the impact energy required to penetrate the laminate. For the round nose shape an impact energy of approximately 32.5J is indicated and for the flat nose shape 40J. The penetration energy levels indicated using the figures provide a crude estimation but do not take into account the effect of reduced flexibility once the back surface

ISSN: 2349 – 4891

plies start to fail. Failure of the back surface plies caused the total absorbed energy to be non-linear as shown by the points appearing on the right. The values from the figures are therefore less than the values recorded during the subsequent impact tests. In the figures, the strain energies were recorded during test. They provide a better picture of the laminate response to the impact event and quite clearly show changes in laminate behaviour. Initially low strain energy levels are recorded as most of the absorbed impact energy is returned to the impactor, which rebounds. A change in response at impact energy of 5J can be seen with increased strain energy for the round and for the flat a sharp increase at 18J is recorded. As damage area verses impact energy this can be attributable to delamination initiation as the critical strain energy is reached [10]. The subsequent propagation energy level is lower than the critical strain energy and therefore rapid growth is seen until the strain energy level drops below the propagation energy threshold. As the impact energy is increased a steadier rate of strain energy absorption is recorded due to minor growth of the delaminations. A second change in strain energy absorption is reached at approximately 13J for the round. The flat response is difficult to distinguish with few impact energy tests beyond 30J but was estimated with aid of impact testing at approximately 30J. This is associated with the back surface ply cracking and subsequent reduction in flexural stiffness. Energy is then absorbed at a steady rate as the impactor is forced through the laminate plies until full penetration.

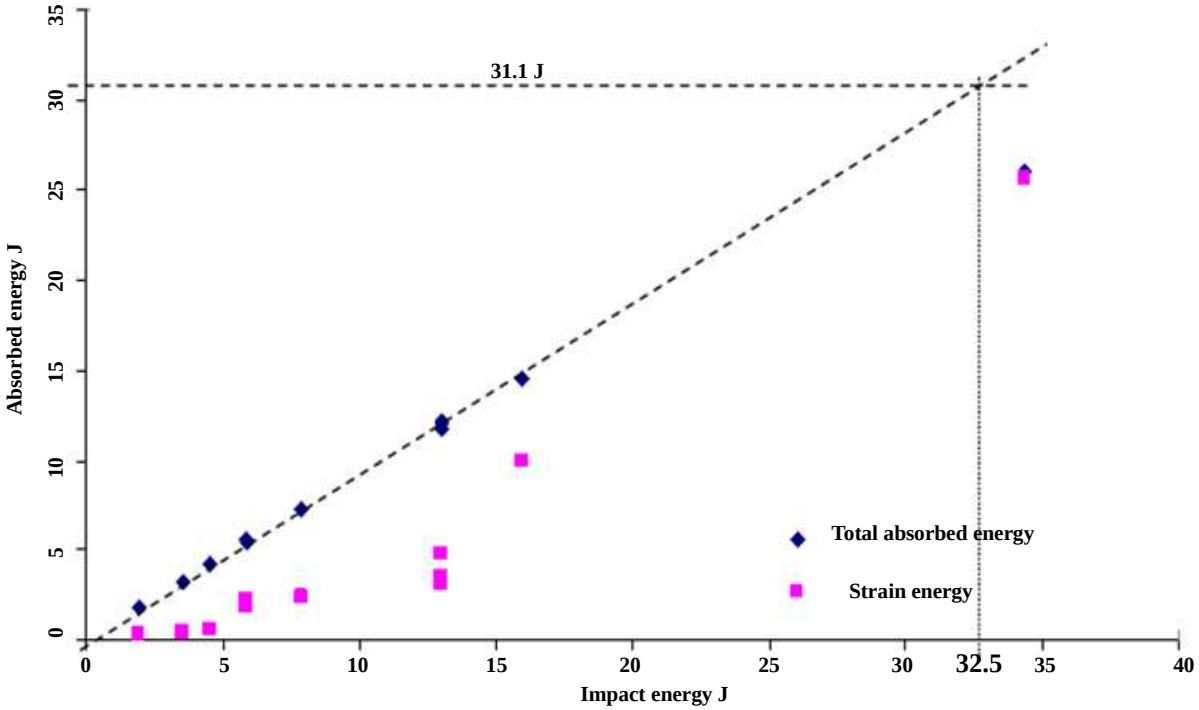

Figure 4: Energy verses impact energy for the round impactor.

ISSN: 2349 – 4891

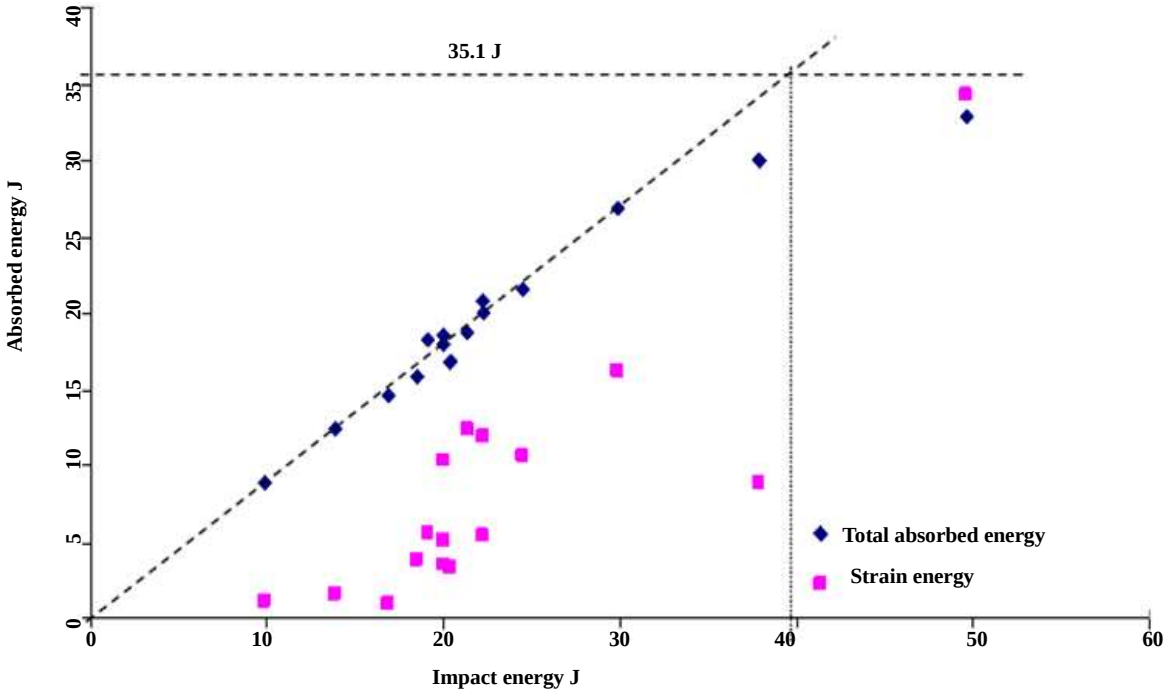

Figure 5: Energy verses impact energy for the round impactor.

5.2 Strain energy versus applied load

The impact results for both the flat and round nose impactors can be seen in figure 6, where the absorbed strain energy is compared to the maximum load obtained during the event. The strain energy presented in the figure is the total absorbed strain energy minus the rebound energy. Therefore the absorbed energy is attributed to the amount of energy used in the creation of damage and some losses due to noise, heat and friction etc. The losses do not have much of an influence on the general trend presented in the **Figure 6**. Three distinct phases can be seen for both impact nose shapes as illustrated in the figure. The first is attributed to matrix cracking of the front surface under the impactor. The second is attributed to the initiation and propagation of delamination and the third is attributable to back surface fracture. The three phases were confirmed with subsequent visual and ultrasonic testing.

ISSN: 2349 – 4891

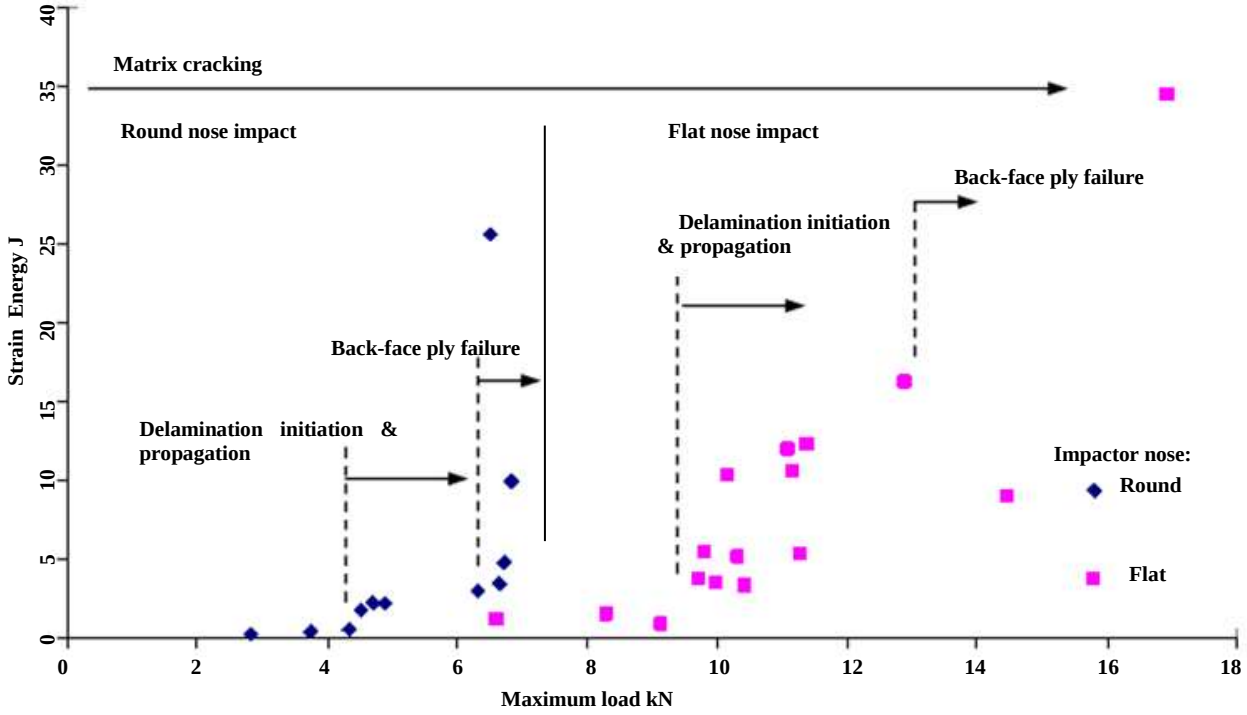

Figure 6: Impact energy verses max load for both impactors.

5.3 Impact energy versus load

As a comparison of results used in the analysis of the impact event the impact energy compared to the maximum load is presented in **Figure 7**. It can be observed that impact energy levels commute up to 9 kN loads after which significant increase can be seen in data points indicating flat nose impacts.

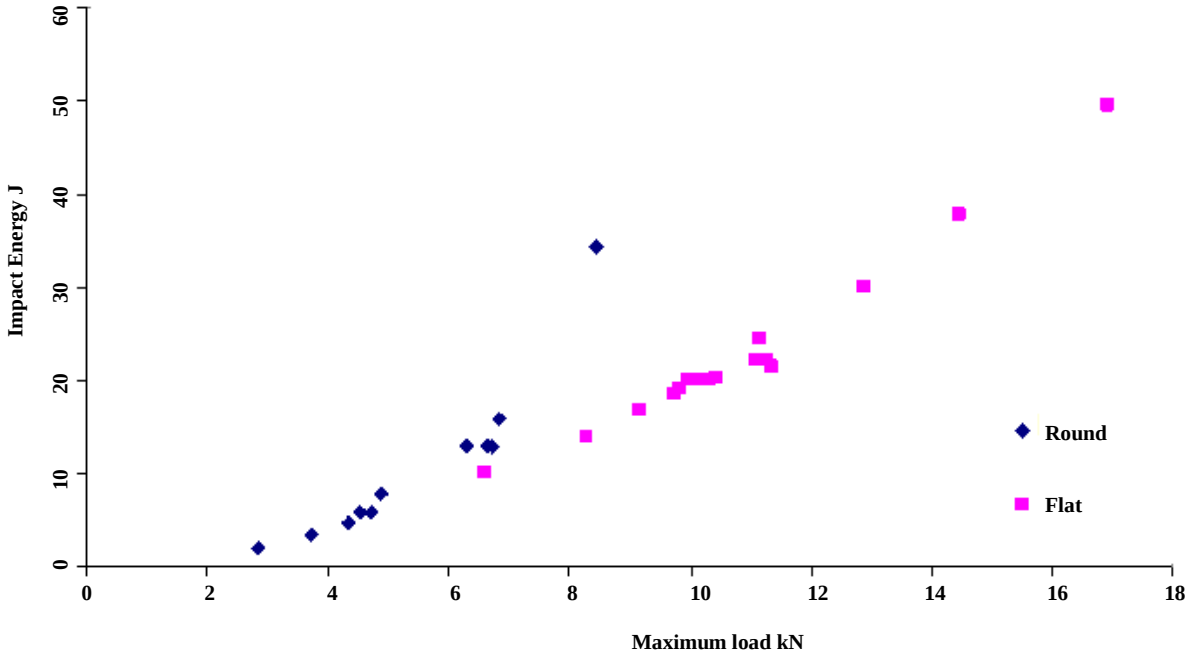

Figure 7: Impact energy versus max load for both impactors

ISSN: 2349 – 4891

5.4 Damage area versus impact energy

A distinct threshold can be seen in **Figure 8** where no damage is observed up to impact energy of approximately 6J under round impactor and under flat nose up to 20 Joules. A second threshold is reached at approximately 13J with a sharp increase in induced damage under nose impactor. This is due to the second failure mode, cracking of the back surface plies. Cracks appear along the fibre direction of the back surface ply, emanating from under the impact site. For flat nose impactor, beyond 20J the laminate rapidly induces damage equating to approximately half the test area as shown in **Figure 9**. On inspection the damage was associated with some matrix cracking of the top surface and with the aid of the c-scan extensive internal delaminations are visible in **Figure 10**.

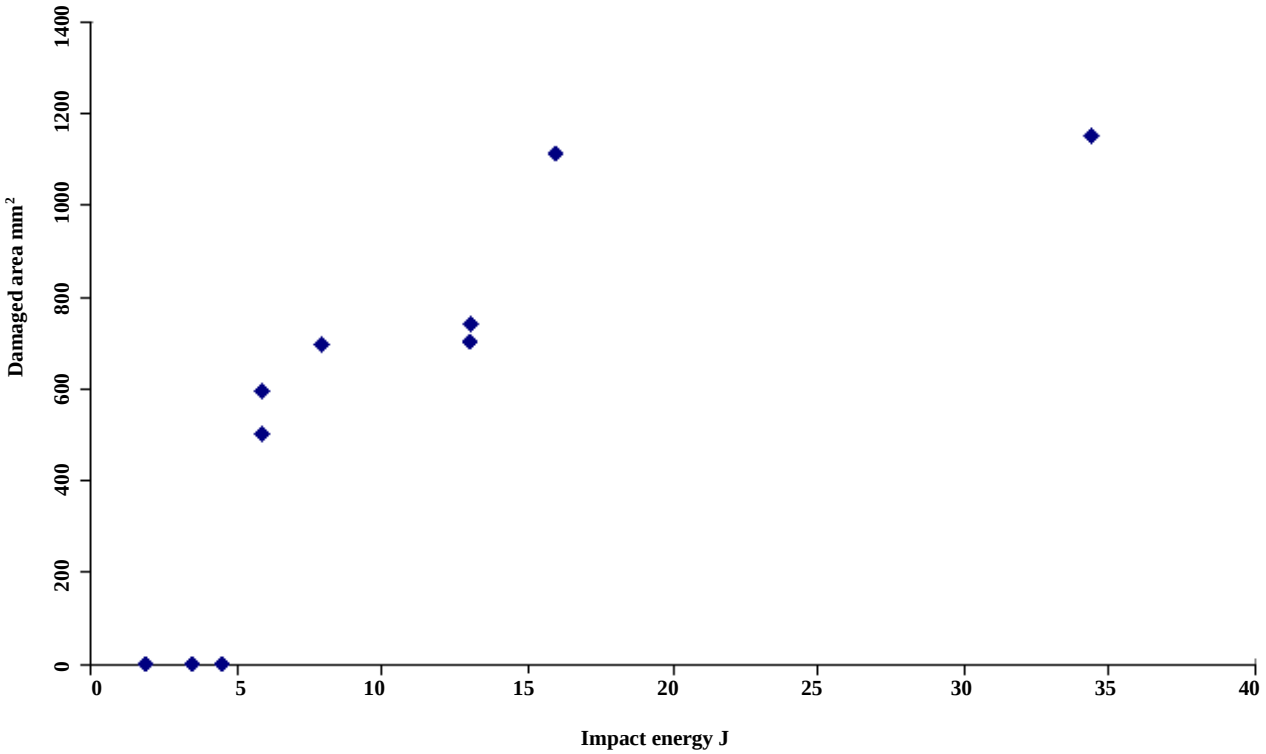

Figure 8: Damage area verses impact energy - round impactor

ISSN: 2349 – 4891

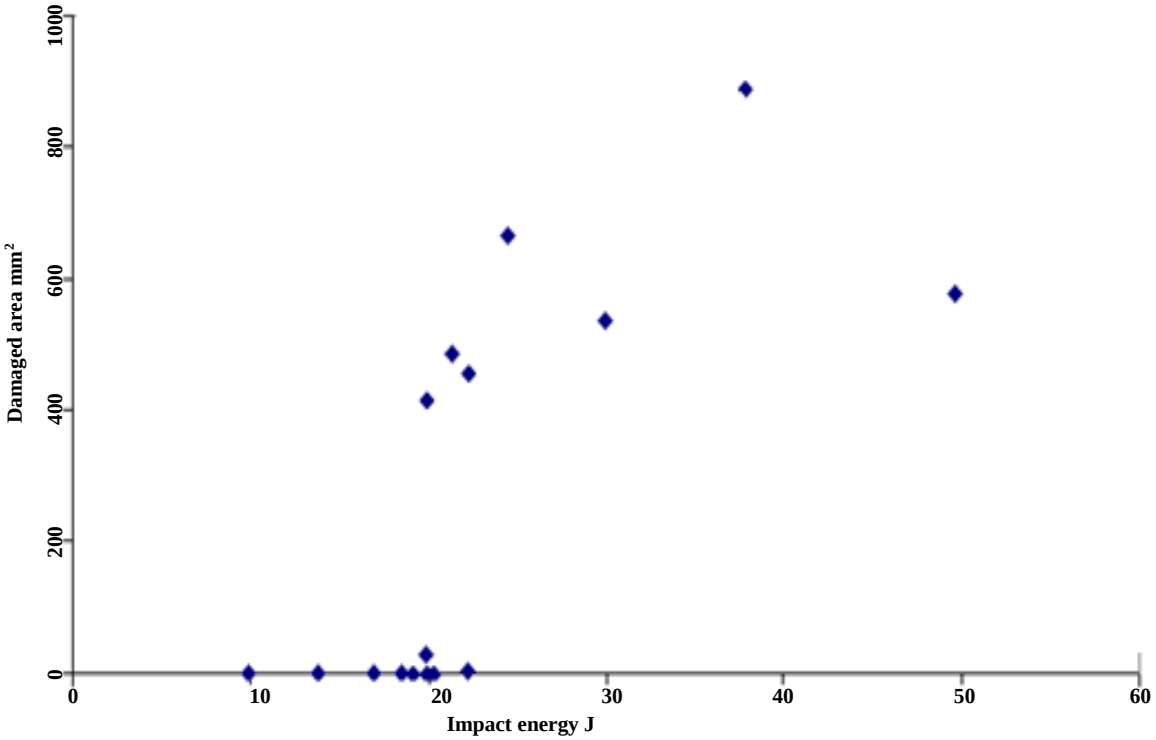

Figure 9: Damage area verses impact energy – flat impactor

A second threshold is reached at approximately 13J with a sharp increase in induced damage. This is due to the second failure mode, cracking of the back surface plies. Cracks appear along the fibre direction of the back surface ply, emanating from under the impact site, which can be seen in **Figure 10(a)**. The cracks sometimes appear in pairs and are greater than a ply thickness, but invariably always follow the direction of the back surface ply. As a consequence of the cracking the laminate has lost most of its structural stiffness and strength. Therefore, indicating that the maximum laminate strength has been reached. The increase in impact energy causes the delaminations to extend to such an extent as to reduce the in-plane stiffness thereby increasing the in-plane stress beyond the ply tensile strength, causing back surface ply fracture. Increasing the impact energy further opens and extends the back surface cracks and the subsequent reduction in stiffness prolongs delamination growth until penetration of the impactor **Figure 10(b)**. Increasing the impact energy further and a separation in the damage response curve is observed. The response seems to separate into lower and upper curves. This could be an indication of different contact force behaviour during impact. If the impactor contacted the laminate squarely then the induced force/strain energy would dissipate over a greater area causing more damage. This could be the reason for the extensive damage, a c-scan image of a specimen impacted with energy of 30J. If the impactor contacted the laminate in an oblique or tilted manner then the induced force/strain energy would be more localised therefore causing more through the thickness damage and consequently appear to have a lower planar damage area.

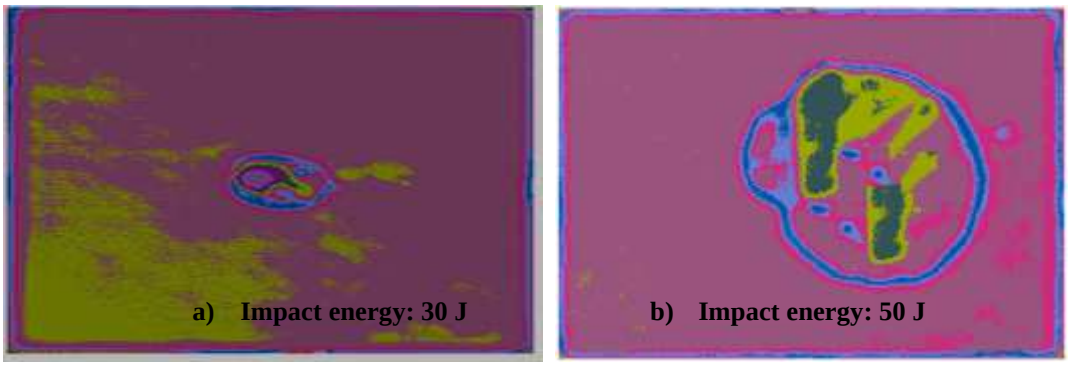

Figure 10: C-scan image of 30J and 50J impacts-round impactor

ISSN: 2349 – 4891

I another test, the final lower point at approximately 50J caused penetration of the laminate, which seems to also indicate a more localised concentration of induced damage. This can be seen in **Figure 11(a)** where the penetration point can be seen in the centre of the c-scan image and also in **Figure 11(b)** a photograph of the impact surface.

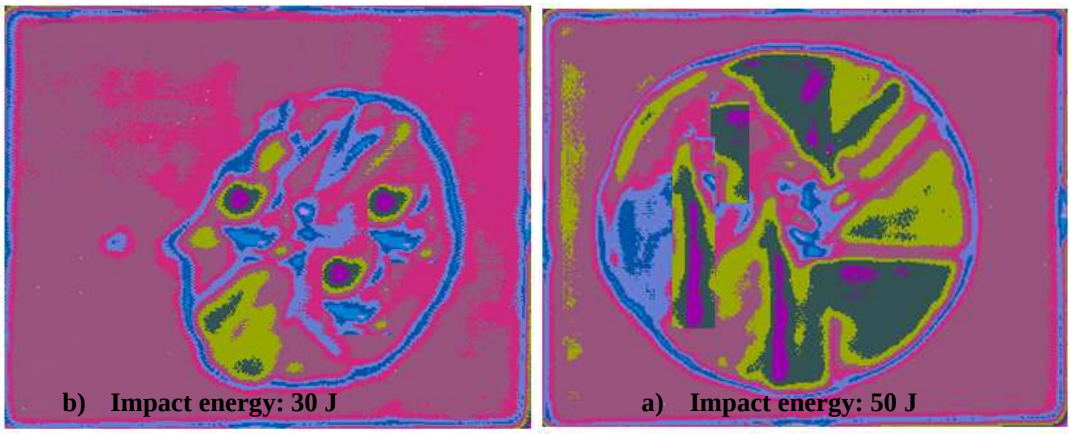

Figure 11: C-scan image of 30J and 50J-flat nose impactor

5.5 Gross damage area versus strain energy

Procedure to approximate the impact induced C-Scan given in [10] was followed. In **Figure 12** the gross damage area is compared to the strain energy used in the creation of the damage and shows an initial rapid increase in damage area at approximately 2.0J. The delamination then propagates at a slower rate as the delamination boundaries propagate further away from the impact site. As the impact energy is increased a limit to the damage sustained is reached. The extension of the delamination boundaries and the back surface fracture reduce the in-plane flexural stiffness and the fracture process reverts from in-plane damage to through the thickness damage.

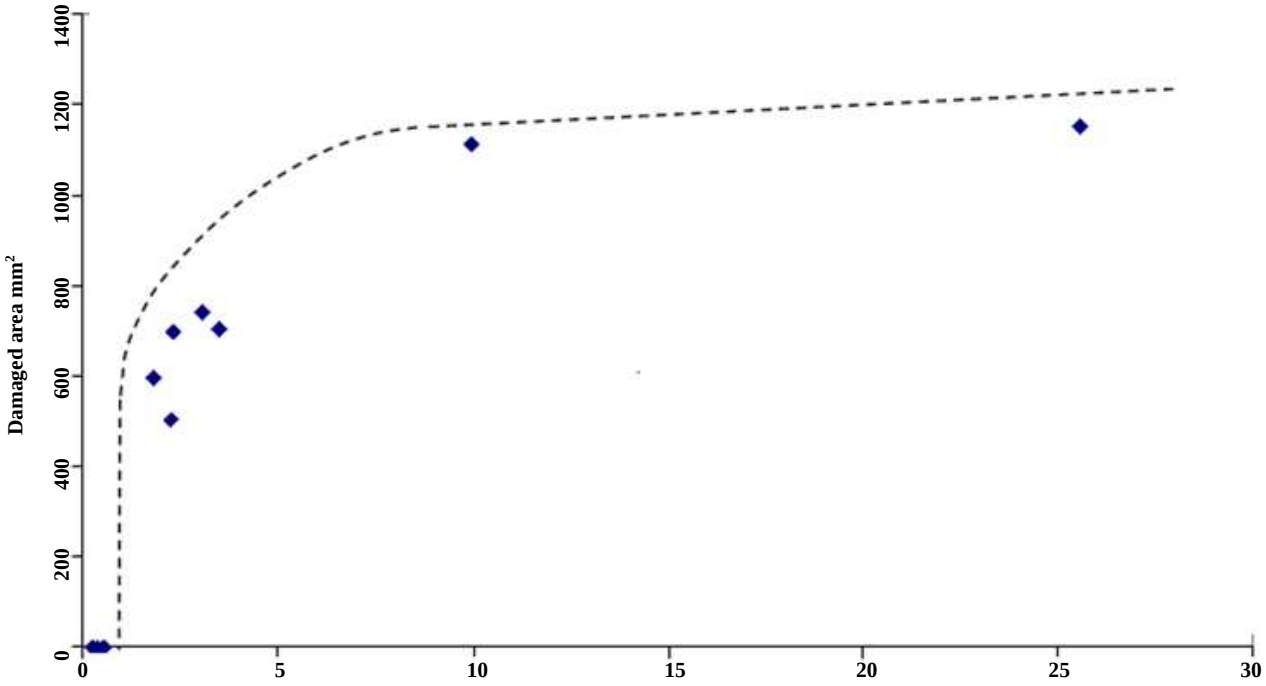

Figure 12: Damage area versus strain energy-round nose impactor

ISSN: 2349 – 4891

Under coupon test conditions it could be said that a maximum damage area exists irrespective of the amount of impact energy applied or strain energy absorbed. A boundary to the results could be drawn (dashed line) where inside the boundary damage will exist and outside damage either does not exist due to the energy level being to initiate delamination or the maximum damage area has already been attained. Under ideal conditions the amount of energy required to initiated delamination, critical strain energy release rate (G_{IIc}) for a particular laminate lay-up and material can be considered a constant, and the amount of damage sustained per strain energy input could be considered linear. The change in rate of damage area per strain energy illustrated by the knee in the dashed line could be related to the contact force. In **Figure 13** the results are presented for gross damage area compared to the strain energy used in the creation of the damage. Once delamination has initiated a distinct step change in damage area can be seen at approximately 9J. This is followed by very slow growth for the amount of strain energy and is associated with the change in dominant damage mechanism from propagating delamination to through the thickness fibre fracture. Some delamination propagation will however continue with delaminations initiating and propagating throughout the thickness of the specimen until failure of the back surface. These remain within the bounds of the original gross damage area and could be quantified with an ultrasonic z-scan (ultrasonic c-scan but concentrated on individual ply layers and then a through the thickness picture is built). Only c-scan was available during the course of this project therefore it wasn't possible to quantify the delaminations on a layer-by-layer basis.

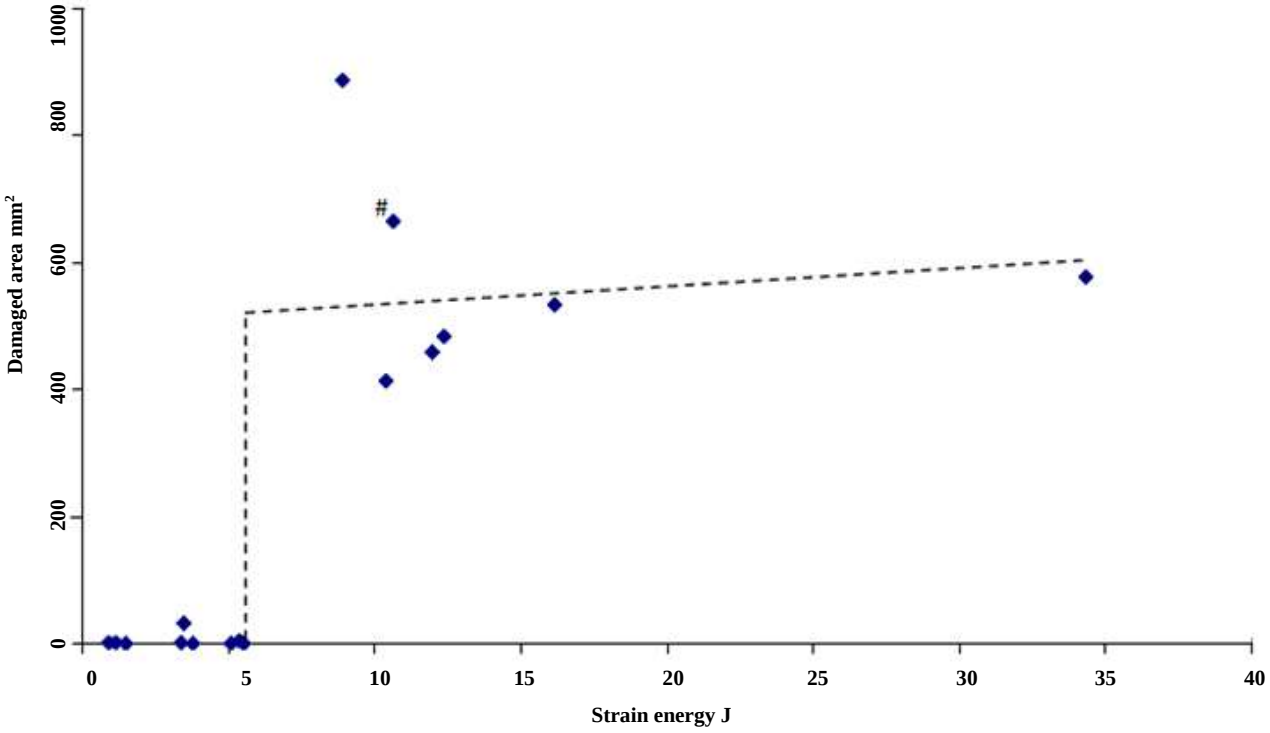

Figure 13: Damage area versus strain energy-flat nose impactor

With the understanding that under coupon test conditions a maximum damage area exists irrespective of the amount of impact energy applied or strain energy absorbed the boundaries in **Figure 12** and **Figure 13** could be considered as test validation limits eliminating the two test results shown in **Figure 13**. These results indicate that for low absorbed strain energy, high damage area is produced, which is not confirmed by the remaining test results. On inspection of the back surface strain levels for specimen hash symbol '#', an unexpected increase was recorded which could be associated with an increase in the flexibility caused by poor specimen clamping.

5.6 Data filtering based on built-in filters and data acquisition system

The examinations of the experimental results were assisted with the use of digital filters. The aim of the filtering was to remove the low frequency impact response of the plate so it would not dominate the high frequency signals. The instrumented filtering is widely used for evaluating the impact damage of composites. The development of photographic techniques for

ISSN: 2349 – 4891

observing the impact process and the recognition that the level of filtering of the force-time signal can significantly affects the results. The ability to monitor force-time signals the course of impact deformation offered considerable potential over tests that merely articulated input energy to a specimen. The first effect is to remove the small oscillations which are observed in the unbroken specimen, and essentially are oscillations of the impactor. At a lower frequency the curve becomes distorted, shifting towards longer times (larger deflections) and is reduced in height. It is clear that too much filtering significantly distorts the signal and that the forces and energies registered are reduced, even in this case where the curve is gently rounded. By taking a set of photographs, each at a different time after the start of impact, it is possible to start to resolve the meaning of different peaks in the force-time curve. This material principally fails by the initiation and growth of a variety of cracks. The material is also stiff and fails at a small stresses and hence small deflections. Signals from the critical regions then give rise to incorrect quantitative data analysis.

5.7

5.7.1 Energy history v impactor nose shape for 8-Ply laminate

The impact velocity for both the impactor nose shape is the same 2.2 m/s. It can be seen from round nose shape curve **Figure 14** that there is no elastic energy under the curve its behaviour is almost stable. However, impact velocity level under flat nose curve has changed considerably. The drop in impact energy from 12 J to 6 J can be attributed to the 50% energy absorbed by the impact from flat nose. This indicates that the gathered and filtered can also predict energy levels particularly the absorbed energy.

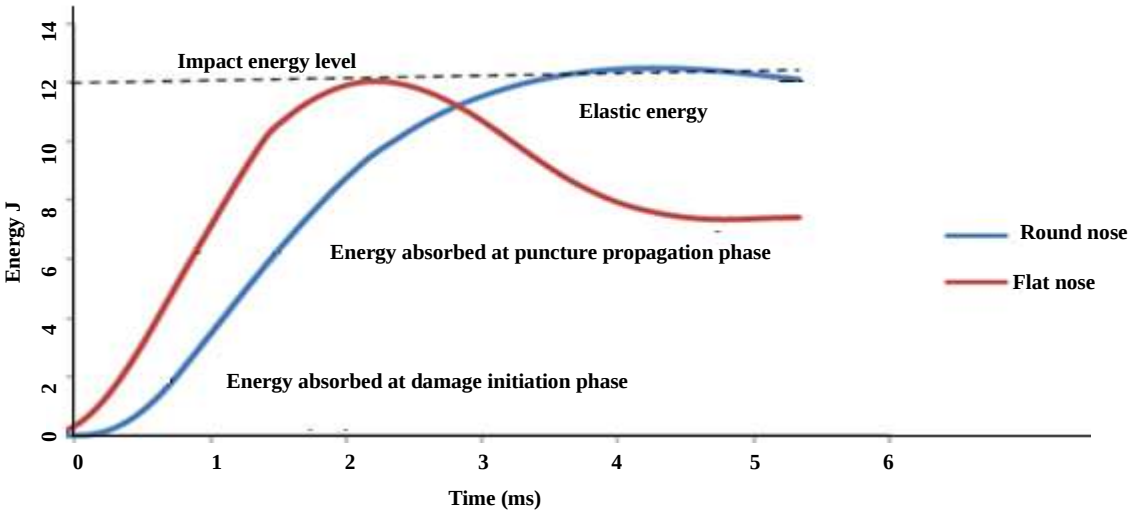

Figure 14: Energy-history plot of 8-ply laminate impacted with round and flat nose impactors

5.7.2 Energy history for 16-Ply laminates

The representative energy history plot of 16-Ply laminate impacted at 3.12 m/s and is shown in

Figure 15. Influence from the impactor nose can be assessed though correlating energy phases to the damage mode shapes. Despite same velocity both the impactor attain different impact energy levels. Contrary to 8-Ply laminate slightly increased impact energy level due to round nose impact. Absorbed energy curve starts increasing after 2 second in the case of impact from flat nose impactor. Both types of impacts have generated approximate absorbed up to 50% of the impact energy. The impact energy curve of the round nose impact drops to 20J which could be approximated to 35% absorbed energy. Impact energy-time curves remain constant. At vibrations and there phases of elastic energies. Impact from round nose depicts smooth trends after one second of the impact time. Influence of the impact from flat nose remains for seven seconds and it finishes after ten seconds. As the contact of the flat nose remains for a longer time period, it therefore, generates more internal damage than the round type of impactor. The curve representing round nose shape shows peak energy level at 27J while peak load for flat nose impactor is indicated at 24J. The absorbed energy curve under flat nose impactor shows these curves, the highest tip of the curve shows maximum impact energy and the end of the curve shows the absorbed energy.

ISSN: 2349 – 4891

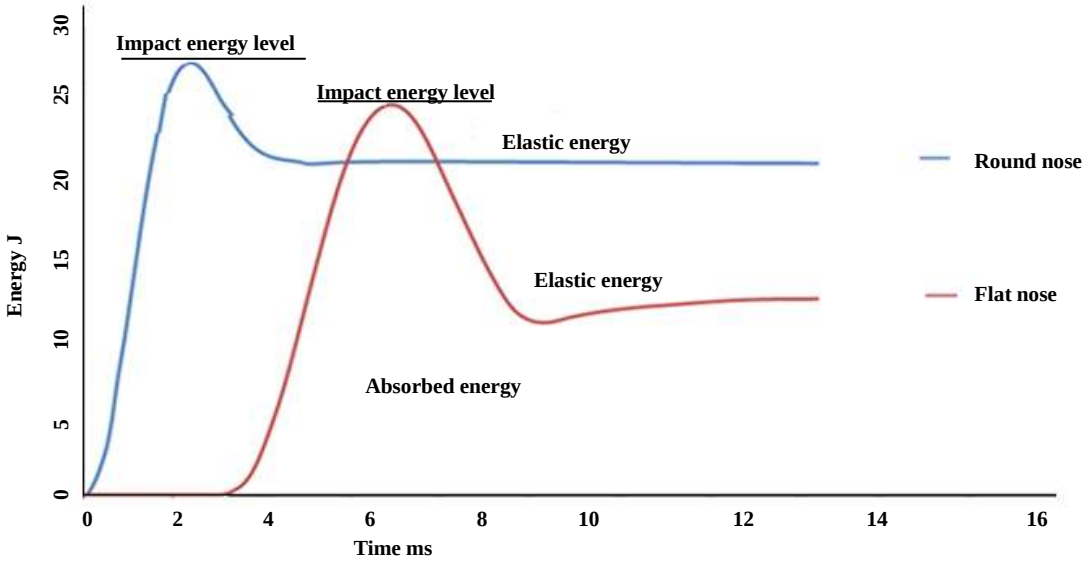

Figure 15: Energy-history plot of 16-Ply laminate impact velocity 3.12m/s

The energy difference between maximum impact energy and absorbed energy are used for rebound of the impactor. For perforation, the energy difference is used for friction between impactor and laminate. In the case of perforation the curves increase without any reduction and finally saturate.

5.8 Data filtering using numerical techniques

Impacts with flat nose of relatively thick laminates produce level off load-deflection curves once a certain displacement/energy is reached as shown in **Figure 16** due to limitations of the testing and data logging systems. The energy-based approach is preferred to employ to quantify the energy absorbed by different mechanisms during flat nose impacts augmented with data filtering and extrapolation techniques. Such advanced data filtering techniques are useful to characterize load thresholds and absorbed energies from the leveled off curves for the determination of the accumulated internal damage (extent of damage). More reliable and robust methods are based on numerical analysis techniques. Extrapolation of numerical values consists of using the curve fitting techniques to estimate data quantities and then extend predictions based upon the estimated data. Curve-fitting of a line calculates a future value by utilising the existing x- and y-values. The new value is predicted by using linear regression. However, the method cannot be applied to filter and extrapolate data herein as the method is based on average values of slopes which are zeros for straight lines. Other widely used algorithms are numerical integrations that could more reliably lead to a band of future quantities. One such method is the modified Simpson's rule regarded as inherent filter. Simpson's rule is a method of finding areas under a curve using an approximate integration method. The next part of Simpson's rule is regression. This results in an equation for velocity that can be used to calculate other values such as displacements by similar integration. Other value that can be obtained from this is the force if mass of free falling weight and the acceleration are known. The modified Simpson's rule given by the 2^{nd} order polynomials (parabolas) Eq. (34) was coded in MATLAB software for approximating the flat nose curve shown in **Figure 16**.

ISSN: 2349 – 4891

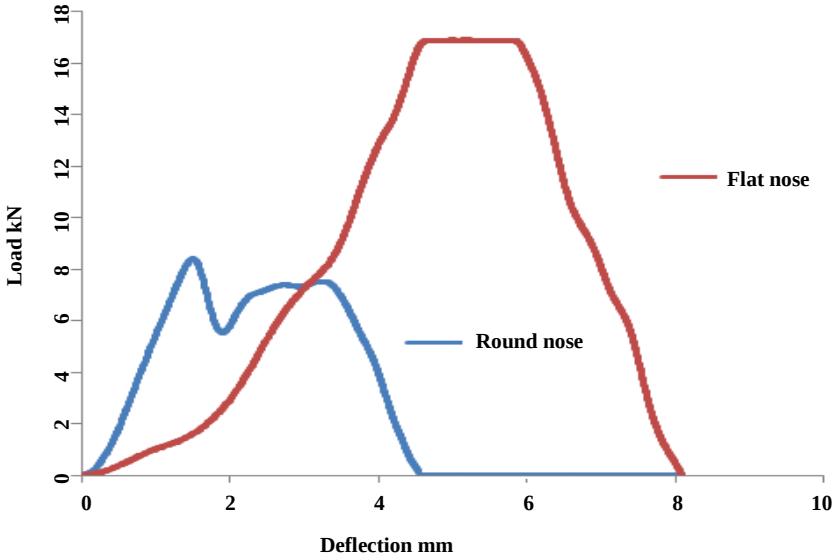

Figure 16: Energy-histories of 16-Ply laminate velocity 3.72 m/s

The energy absorbed by the laminate during impact can be quantified by evaluating the area under the curve. Area under the load-deflection curve was numerically integrated using Simpson's modified rule Eq. (34) to estimate impact energy. The numerical integration of the areas under the curve produce energy estimates 21J for unfiltered values and 26J from the flat nose filtered values using the Eq. (34) for 16-Ply laminate shown in **Table 2**.

Table 2: **Numerical integration to estimate area under the curve**

Deflection mm	Round Impactor	Flat Impactor		Simpson's multiplier	Area under the curve J	
	Load kN	Load kN	Filtered Load kN		Unfiltered	Filtered
0.25	0	.6	.6	1	0.6	0.6
0.5	1	1.6	1.6	4	0.64	0.64
0.75	2	2.1	2.1	2	0.42	0.42
1	3	3.	5.6	4	2.24	2.24
1.25	4	4	7.6	2	15.2	15.2
1.5	5	4.5	8.4	4	33.6	33.6
1.75	6	5.2	10.2	2	204	204
2	7	6	13	4	52.0	52.0
2.25	7.5	6.5	14	2	28.0	28.0
2.5	8	7	16	4	64.0	64.0
2.75	8.5	7.8	20.1	2	32.0	40.
3	9.	8.6	18.1	1	16.0	18.08
			Energy J		**21.23**	**26.1**

Similarly, for another test of relatively higher energy of 50J, areas under the curve produce energy estimates 30J for unfiltered values and 46J from the flat nose filtered values when moving average extrapolation techniques [10] were applied. The results indicate that numerical integration coupled with statistical moving average methods could predict acceptable estimate of absorbed energy values from the impact recorded clipped/leveled off data.

ISSN: 2349 – 4891

4 Conclusions

In this work, the initiation, propagation, and extent of damage in laminates subjected to round and flat nose profiles were investigated using analytical and data filtering approach. Theoretical relationships of parameters were complemented with data filtering and data extrapolation techniques to predict reliable absorbed energy quantities. Based on comparison of the results, the following conclusions were drawn:

a) Absorbed energy versus impact energy levels show damage initiation, propagation, and extent as expected
b) Strain energy versus maximum load separate difference damage regions under impactor nose profiles
c) Impact energy versus maximum applied load show significant difference under both the nose profiles with acceptable agreement to the available c-scans
d) Impact induced damage areas versus strain energy show ranges of damage levels obtained with strain energy levels used in deformation under both the impactor nose profiles
e) Energy-time history plots of 8- and 16-Ply laminates agree well against the available data
f) Data filtering and data extrapolation techniques predicted extent of impact induced damage from leveled off curves

The damage process of individual ply can also be reconstructed from comparing the corresponding load–deflection curves, energy profiles, and images of damaged specimens. The same work and methodology could be efficiently modified and applied to approximate extent of the impact induced internal damage of similar cases.

References

[1] James RA. Impact damage resistance and damage tolerance of fibre reinforced laminated composites (Ph.D. thesis), University of Bolton, United Kingdom, 2006.

[2] Caprino G, Lopresto V, Scarponi C, Briotti G. Influence of material thickness on the response of carbon–fabric/epoxy panels to low velocity impact. Compos Sci Technol 1999;59:2279–86.

[3] Hosur MV, Adbullah M, Jeelani S. Studies on the low-velocity impact response of woven hybrid composites. Compos Struct 2005;67:253–62.

[4] Datta S, Krishna AV, Rao RMVGK. Low velocity impact damage tolerance studies on glass/epoxy laminates–effects of material, process and test parameters. J Reinf Plast Compos 2004;23(3):327–45.

[5] Hosseinzadeh R, Shokireh MM and Lessard L. Damage behaviour of fibre reinforced composite plates subjected to drop weight impacts. Compos Sci Technol 2005; 66:61-68.

[6] Mitrevski T, Marshall IH, Thomson RS and Jones R. Low-velocity impacts on preloaded GFRP laminates with various impactor shapes. Compos Struct 2006;76:209-217.

[7] Deng Y, Zhang W, Cao Z. Experimental investigation on the ballistic resistance of monolithic and multi-layered plates against hemispherical-nosed projectiles impact. Mater Des 2012;41:266–81.

[8] Abrate S. Impact on composite structures. Cambridge: Cambridge University Press; 1998.

[9] Cantwell WJ, Morton J. The impact resistance of composite materials – a review. Composites 1991;22:347–62.

[10] Umar Farooq, Finite Element Simulation of Flat Nose low Velocity Impact Behaviour of Carbon Fibre Composite Laminates (Ph.D. thesis), University of Bolton, United Kingdom, 2014.

[11] Ercan S, Benjamin L, Feridun D. Drop-weight impact response of hybrid composites impacted by impactor of various geometries. Mater Des 2013;52:67-77.

[12] Deng Y, Zhang W, Cao Z. Experimental investigation on the ballistic resistance of monolithic and multi-layered plates against hemispherical-nosed projectiles impact. Mater Des 2012;41:266-81.

[13] Farooq U, Peter Myler P. Ply level failure prediction of carbon fibre reinforced laminated composite panels subjected to low velocity drop-weight impact using adaptive meshing techniques. Acta Astronautica 2014;102:169–177.

[14] Farooq U, Peter Myler P. Finite element simulation of buckling-induced failure of carbon fibre-reinforced laminated composite panels embedded with damage zones. Acta Astronautica 2015;115:314–329.

[15] Farooq U, Myler P. Flat nose low velocity drop-weight impact response of carbon fibre composites using non-destructive damage detection. DE GRUYTER Open Eng. 2015; 5:131–147.

[16] Farooq U, Myler P. Finite simulation of carbon fibre-reinforced composite laminates subjected to low velocity impact using damage induced static load-deflection methodology. Thin-walled structures 2015;97:63-73.

[17] Farooq U, Myler P. Prediction of load threshold of fibre-reinforced laminated composite panels subjected to low velocity drop-weight impact using

efficient data filtering techniques. Results in Physics 2015;5:206-221.

[18] Farooq U, Peter Myler P. Ply level failure prediction of carbon fibre reinforced laminated composite panels subjected to low velocity drop-weight impact using adaptive meshing techniques. Acta Astronautica 2014;102:169–177.

[19] Todoroki A, Tanaka M and Yoshinobu S. Multi-prove electric potential change method for delamination monitoring of graphite/composite plates using normalized response surfaces. Compos Sci Technol 2004;62:749-758.

[20] Hoshikawa H and Koyama K. A new Eddy-current probe with minimal liftoff noise and phase information on discontinuity depth. Mater Evaluation 2003; 61(3):423-427

[21] Farooq U, Myler P. Efficient computational modelling of carbon fibre reinforced laminated composite panels subjected to low velocity drop-weight impact. Mater Des 2014;54: 43–56.

[22] Mariani S and Corigliano A. Impact induced composite delamination: state and parameter identification via joint and dual extended Kalman filters. Comput Method Appl Mech Eng 2005;194: 5242-5272.

[23] Mariani S and Ghisi A. Unscented Kalman filtering for nonlinear structural dynamics. Nonlinear Dyn 2007;49:131-150.

[24] Stefano Mariani. Failure Assessment of layered composites subject to impact
loading: a Finite Element, Sigma-Point Kalman filter approach failure assessment approach. Algorithms 2009;2:808-827.

[25] Julier S, Uhlmann J and Durrant-Whyte H. A new method for the nonlinear transformation of means and co-variances in filters and estimators. IEEE Trans. Automat. Control 2000;45:477-482.

[26] Ott R, Lyman L, Michael. An introduction to statistical methods and data analysis (6^{th} ed.). Brooks/Cole, Cengage Learning, 2008.

[27] Jie W, Fred KC and Zhenhai X. Wavelet de-noising in electrical resistance based damage detection of carbon fibre composite materials. J Mater Sci Research 2013;2(1):82-100.

[28] Yan YJ and Yam LH. Online detection of crack damage in composite plates using embedded piezoelectric actuators/sensors and wavelets analysis. Comput Struct 2002; 58(1): 29-38.